Anal Bioanal Chem (2010) 398:3051–3061
DOI 10.1007/s00216-010-4283-6

ORIGINAL PAPER

Raman chemical mapping reveals site of action of HIV protease inhibitors in HPV16 E6 expressing cervical carcinoma cells

Dong-Hyun Kim · Roger M. Jarvis · J. William Allwood · Gavin Batman · Rowan E. Moore · Emma Marsden-Edwards · Lynne Hampson · Ian N. Hampson · Royston Goodacre

Received: 17 August 2010 / Revised: 28 September 2010 / Accepted: 29 September 2010 / Published online: 19 October 2010

Abstract It has been shown that the HIV protease inhibitors indinavir and lopinavir may have activity against the human papilloma virus (HPV) type 16 inhibiting HPV E6-mediated proteasomal degradation of p53 in cultured cervical carcinoma cells. However, their mode and site of action is unknown. HPV-negative C33A cervical carcinoma cells and the same cells stably transfected with E6 (C33AE6) were exposed to indinavir and lopinavir at concentrations of 1 mM and 30 μM, respectively. The intracellular distribution of metabolites and metabolic changes induced by these treatments were investigated by Raman microspectroscopic imaging combined with the analysis of cell fractionation products by liquid chromatography–mass spectrometry (LC-MS). A uniform cellular distribution of proteins was found in drug-treated cells irrespective of cell type. Indinavir was observed to co-localise with nucleic acid in the nucleus, but only in E6 expressing cells. Principal components analysis (PCA) score maps generated on the full Raman hypercube and the corresponding PCA loadings plots revealed that the majority of metabolic variations influenced by the drug exposure within the cells were associated with changes in nucleic acids. Analysis of cell fractionation products by LC-MS confirmed that the level of indinavir in nuclear extracts was approximately eight-fold greater than in the cytoplasm. These data demonstrate that indinavir undergoes enhanced nuclear accumulation in E6-expressing cells, which suggests that this is the most likely site of action for this compound against HPV.

Keywords HPV · Indinavir · Lopinavir · Raman chemical mapping · LC-MS

Electronic supplementary material The online version of this article (doi:10.1007/s00216-010-4283-6) contains supplementary material, which is available to authorized users.

D.-H. Kim · R. M. Jarvis · J. W. Allwood · R. Goodacre
School of Chemistry, Manchester Interdisciplinary Biocentre,
The University of Manchester,
131 Princess Street,
Manchester M1 7DN, UK

G. Batman · L. Hampson · I. N. Hampson
Gynaecological Oncology Laboratories,
School of Cancer & Enabling Sciences, St Mary's Hospital,
The University of Manchester,
Manchester M13 9WL, UK

R. E. Moore · E. Marsden-Edwards
Waters Corporation,
Atlas Park, Simonsway,
Manchester M22 5PP, UK

R. Goodacre (✉)
Manchester Centre for Integrative Systems Biology (MCISB),
Manchester Interdisciplinary Biocentre,
The University of Manchester,
131 Princess Street,
Manchester M1 7DN, UK
e-mail: roy.goodacre@manchester.ac.uk

Introduction

Globally, an estimated 493,000 women are affected by cervical cancer resulting in a staggering 273,500 deaths each year (National Cervical Cancer Coalition; www.nccc-online.org). Indeed, in many low-resource countries, it is the greatest cause of women's cancer-related mortality. Human papilloma virus (HPV) is the major cause of cervical cancer [1], and there are >120 different types of HPV associated with a variety of clinical lesions [2]. There are approximately 13 so-called high-risk types which are associated with cervical cancers [1, 3], although HPV16

and 18 are the most prevalent high-risk types, accounting for >60% of cases [4, 5].

Surgery is currently the treatment of choice for HPV-related pre-cancerous cervical intraepithelial neoplasia [4, 6]. However, since it carries an increased risk of infertility, this is restricted to high-grade disease [7].

Many countries are implementing prophylactic anti-HPV vaccination programmes, yet these primarily protect against types 16 and 18 only, which leaves a significant proportion of high-risk HPV-related disease unprotected. Furthermore, vaccination is most effective when given to women prior to HPV infection, and it is expensive. Thus, since cervical cancer can take from 10 to 20 years to develop, persistently infected women will still be at risk for many years, particularly in low-resource countries that cannot afford vaccination. It is also notable that such countries do not have routine cervical screening services. Thus, it is clear that a low-cost, self-applied treatment for HPV-related disease would have many benefits, particularly in low-resource settings.

The E6 and E7 viral oncoproteins from high-risk types of HPV are responsible for their oncogenic properties, and their continued expression is essential for the growth and survival of HPV transformed cells [8]. We have previously shown that the anti-HIV protease inhibitors (HIV PIs) indinavir and lopinavir inhibit E6-mediated proteasomal degradation of p53 and selectively kill E6-dependant cervical carcinoma cells *in vitro* [9]. We have also recently shown that these compounds cause very specific alterations in the metabolism of cultured E6-expressing cervical carcinoma cells [10]. Indeed, anti-HIV drugs are now becoming increasingly recognised as having significant off-target antineoplastic properties [11]. However, the site and mode of action of this type of drug with respect to HPV is unknown. In order to address this question, we used Raman microspectroscopic imaging to investigate changes in the intracellular distribution of metabolites and macromolecules, and the subcellular location of indinavir and lopinavir in control cervical carcinoma cells treated with these compounds.

Materials and methods

Cell line and culture medium

HPV-negative human C33A cervical carcinoma cells were maintained in RPMI 1640 (Invitrogen, Paisley, UK) supplemented with 10% foetal bovine serum and 2 mM L-glutamine (Sigma-Aldrich Company Ltd., Dorset, UK; complete medium) at 37 °C, 5% CO_2. C33A cells stably transfected with HPV16 E6 (termed "C33AE6") and the pcDNA3.1 control vector (termed "C33AV") were derived and cultured as previously described [12].

Protease inhibitor

Indinavir was obtained through the NIH AIDS Research and Reference Reagent Program (Division of AIDS, NIAID, NIH): indinavir sulphate (8145). Lopinavir was provided as a generous gift from Abbott Laboratories (Park Road, Abbott Park, IL 60064-6187, USA). Indinavir and lopinavir were dissolved in sterile distilled water and DMSO (Sigma-Aldrich Company Ltd.), respectively, at a working stock concentration of 20 mM.

Raman sample preparation

Each 1×10^6 of C33AV and E6 cells was seeded in T75 culture flasks with 20 mL of the complete medium and then incubated at 37 °C, 5% CO_2. Prior to confluence, the medium was removed and the cells were detached by trypsinisation for 3 min at 37 °C, 5% CO_2. Following this, 2×10^4 cells were seeded onto a single CaF_2 disc (Crystran Plc, Dorset, UK, 20-mm diameter×2-mm thickness) in 3 mL of the complete medium in a six-well culture dish and allowed to adhere overnight at 37 °C, 5% CO_2. Previous work [9] reported dose-dependent experiments on the HIV protease inhibitors indinavir and lopinavir to inhibit the degradation of p53 promoted by E6. Based on this study, cells were then treated with either 1 mM of indinavir, 30 μM of lopinavir, water or DMSO (as controls) and incubated for 24 h at 37 °C, 5% CO_2. The cells were subsequently fixed in ice-cold methanol for 4 min at −20 °C, then washed and stored in phosphate-buffered saline (PBS) at 4 °C until use.

Raman microspectroscopy and data analysis

Raman point spectra for the chemical maps were obtained on a Renishaw System 2000 Raman microscope (Renishaw Plc., Old Town, Wotton-under-Edge, Gloucestershire, UK), and spectra were recorded directly on single CaF_2 disc mounted cells. All cells were mounted in PBS under coverslips during the acquisition of spectra to avoid desiccation. An 830-nm NIR diode laser was used for excitation, with laser power of ~5 mW at the sample using a ×50 microscope objective, with 0.95 NA which resulted in ~0.75-μm lateral spatial resolution. At each location (or pixel), a Raman spectrum was acquired over the region from 400 to 2,000 cm^{-1}. The stage was then moved in 1-μm steps for each acquisition, with the overall result generating a 3D hypercube over the single cell of dimensions X *vs.* Y *vs.* Raman spectra (see Electronic supplementary material (ESM) Fig. S1). Spectral acquisition was performed using GRAMS WiRE software (Galactic Industries Corp., Salem, NH, USA) and data processing was carried out with Matlab 7 (The MathWorks, Inc., Natick, MA, USA). Chemical

image maps were generated against a variety of univariate metrics, including peak area and S/N ratios with the full process illustrated in Fig. 1.

Matlab was also used to perform principal components analysis (PCA) using the NIPALS (nonlinear iterative partial least squares) algorithm [13]. PCA is a multivariate technique that is used widely to reduce the dimensionality of complex spectroscopic data from many wavenumber assignments to a few principal components (PCs), which retain the majority of variance within the data [14, 15]. Upon collection, the individual spectral data cubes were concatenated to produce a single large dataset within Matlab which was subjected to PCA. The first few PCs were extracted as these explained the majority of the variance and lower ones are likely to contribute only noise. Image maps were constructed from plotting each of the PC scores individually. The data cube was reshaped (in order to plot each PC as a function of X and Y) and PC scores false colour coded to generate chemical maps; the corresponding PC loadings were plotted for the first few scores.

Subcellular fractionation of C33AE6 cells

C33AE6 cells were treated with 0.3 mM of indinavir for 24 h and detached as described in "Raman sample preparation". These were resuspended in complete medium and washed twice with PBS. Cytoplasmic and nuclear extracts were prepared by the use of the NE-PER kit (Pierce, USA) according to the manufacturer's protocols.

Western immunoblotting of sub-fractionated samples

Western immunoblotting was carried out as described in [9, 16] loading 25 μg of each extract per track. Anti-histone deacetylase (HDAC1, Cell Signalling Technology, UK) was used at 1:800 and GAPDH (Abcam, UK) at 1:1,000. Following washing, membranes were incubated with 1:2,000 of HRP-conjugated secondary antibody and visualised with ECL and Hyperfilm (GE Healthcare Life Sciences, Buckinghamshire, UK).

LC-MS analysis of cell sub-fractions

Yields of 1,055 μL of cytoplasmic and 500 μL nuclear fractions were obtained, which reflect the nucleus/cytoplasmic ratio for these cell lines. Aliquots (25 μL) of these extracts were treated with 5 volumes of cold acetone for 1 h at −20 °C, centrifuged at 14,500×*g* for 15 min and the supernatant recovered. These were then dried by speed vacuum concentration for approximately 1 h at 45 °C to reduce the samples to their original volume of ~25 μL.

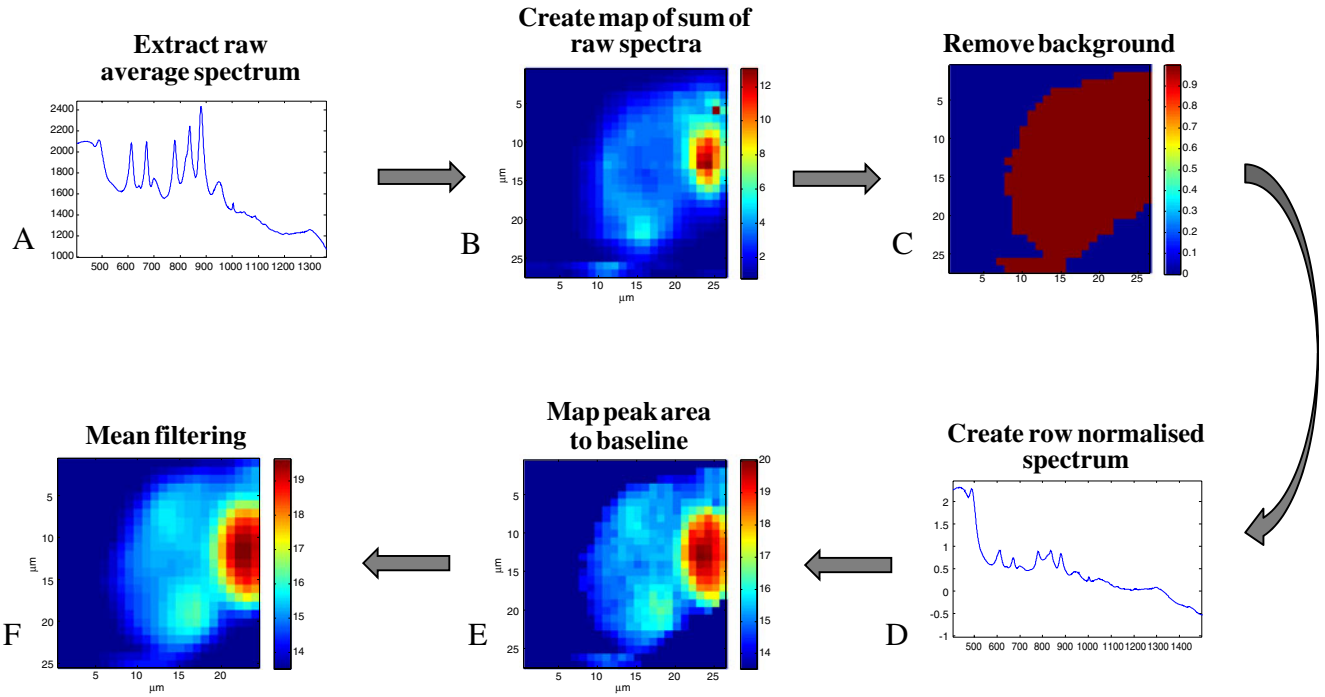

Fig. 1 Process of the generation of chemical image maps. **a** The average spectrum is plotted by the mapping function so that peaks can be selected interactively. **b** Taking the total area under the spectrum and plotting as a 2D image map allows the identification of the cell against the substrate background. **c** A simple threshold is then applied to select pixels/spectra from the map that represent the cell position. **d** The data are reanalyzed minus the background substrate spectra. **e** This can be performed through the integration of peak areas, PCA mapping or alternative algorithms. **f** The resultant image can be further smoothed by applying a 2D moving filter window

A 10-min LC methodology using 10 mM ammonium formate, pH 9, as mobile phase A and acetonitrile as mobile phase B was performed with an Acquity UPLC™ (Waters Ltd., Manchester, UK). A 2-μL sample injection was made onto a 2.1×10-mm HSS T3 (C18) Acquity column held at 45 °C; the mobile phase flow rate was 0.6 mL/min. The following gradient elution was employed (time (min), %B): (0, 2), (8, 98), (8.6, 100), (9.1, 2).

A Xevo™ QTof (Waters Ltd.) MS instrument was used in electrospray ionisation (ESI) positive ionisation mode. Prior to sample analysis, the instrument was calibrated with sodium formate following the instrument setup wizards. Sample data were acquired in MS^E mode [17, 18] with a 0.05-s scan time; the lockspray standard applied was leucine enkephalin (Leu Enk) and two points were employed for lockmass: *m/z* 556.2771 and a fragment ion from Leu Enk *m/z* 120.0813. ESI was operated using an extraction cone voltage of +3 V, a sampling cone voltage of +45 V, and the capillary voltage was set at +3 kV. The source and desolvation temperatures were 120 and 400 °C, respectively, and the cone and desolvation gas flow rates were 20 and 800 Lh^{-1}, respectively. Data were acquired over the *m/z* range 50–1,000 with six biological replicate samples to account for analytical variability.

Results

Raman analysis of C33AV control cells

A representative population of C33AV cells exposed to 1 mM of indinavir or 30 μM of lopinavir were imaged by Raman microspectroscopy. The average spectra for drug-treated and control untreated cells are shown in Fig. 2, which also shows peak centres. Cellular components such as proteins, lipids, nucleic acids and carbohydrates all contribute to this type of analysis, as illustrated in Table 1. As can be seen in Fig. 2 and Table 1, the band at 1,004 cm^{-1} originates from the aromatic ring vibration of phenylalanine and is characteristically observed in biological samples.

Chemical maps of drug-treated C33AV and untreated control cells were employed to analyse and visualise the biochemical distribution of the above intracellular components. White light images, which were used to provide information on the cell shape, and the Raman chemical image maps of cells are shown in Fig. 3. In order to enhance the detection of relevant biological information, CaF_2 substrate background removal was carried out before the image maps were generated (as illustrated in the schematic in Fig. 1). These chemical maps were generated with a spatial resolution of 1 μm from the peak area to baseline of each band within the Raman spectra acquired

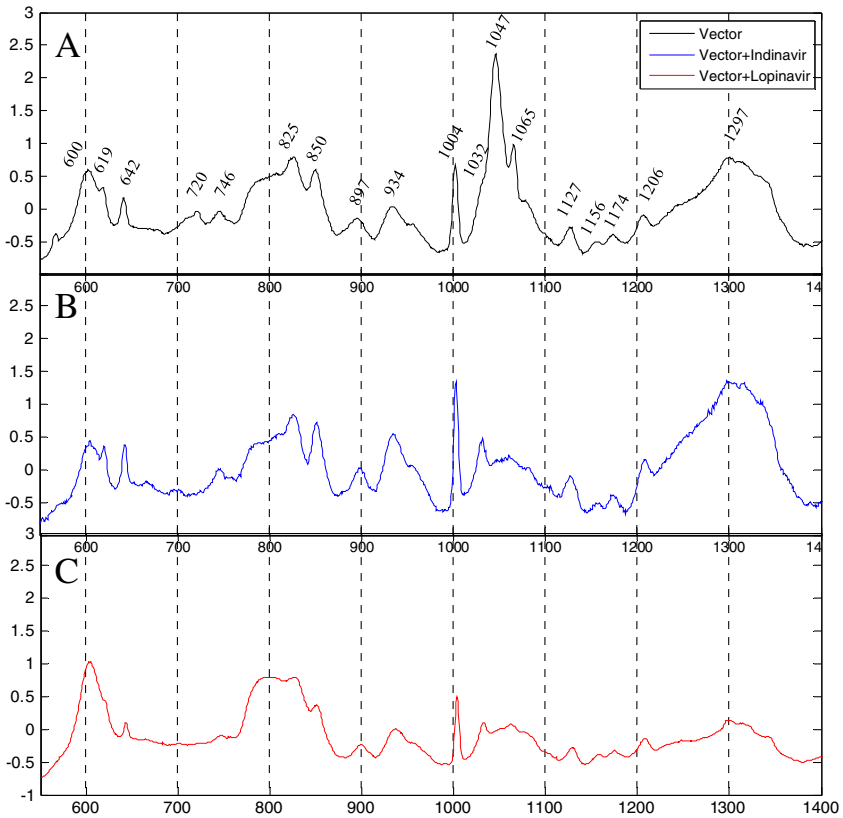

Fig. 2 Mean normalised Raman spectra from vector control cell (C33AV) (**a**) and vector cells exposed to indinavir (**b**) and lopinavir (**c**)

Table 1 Tentative Raman band assignments for the C33A cells

Wavenumber (cm^{-1})	Assignment	Raman vibrational modes
642	Tyr (643)	C–C twist
670	T, G (669)	
680	G	
712	Unidentified	
746	T	
780	C, U, T (782)	
792	C, T	n: (O–P–O) backbone
825		n: (O–P–O) backbone (828)
836	(O-P-O), Tyr (834)	n: RP; n: (O–P–O)
850		p: (C–CH) aromatic def. (852)
890		n: (O–P–O) backbone (898)
		p: (C–C) skeletal modes (898)
934		p: (C–C) backbone str. (937)
948	Deoxyribose (950)	
1003-4	Phe	(C–C) aromatic ring str.
1032	Phe	protein: (C–N) str.
1047	Carbohydrate (1049)	(C–O) str.
1063		p: (C–N) str.; l: chain (C–C) str.
1086		n: (O–P–O) backbone (1088); p: (C–C) skeletal modes (1086)
1109		n: (O–P–O) backbone (1106)
1128, 1133		p: (C–N) str.; l: chain (C–C) str. (1129)
1156		p: (C–C/C–N) str. (1158)
1172, 1174	Tyr, Phe (1175)	(C–C) str. (1172)
1206	Phe, Tyr, Amide III (1209)	
1256	Amide III(1254); C, A (1255)	
1297		(CH_2) def.
1341	A, G (1342)	p: (CH) def. (1342)

Parenthesised numbers, original Raman shifts from [33, 37, 38]

Tyr tyrosine, *Phe* phenylalanine, *A* adenine, *T* thymine, *G* guanine, *C* cytosine, *U* uracil, *RP* reverse primer, *str.* stretching, *def.* deformation, *p* protein, *l* lipid, *n* nucleotide

from the cell and surrounding area. The intense red regions indicate a higher concentration of a chemical constituent(s) relative to the low-intensity signal recorded from the CaF_2 disc substrate, which is represented by blue-coloured pixels.

Raman analysis of C33AE6 cells

The average spectra of C33AE6 and drug-exposed C33AE6 cells are shown in Fig. 4a–c. Since the expression of HPV16 E6 subverts the function of the 26S proteasome to degrade the p53 tumour suppressor and other cellular proteins [1, 3, 19, 20], it is predicted that the intracellular composition of C33AE6 cells will be different from those of the vector cells. As expected, the average spectrum obtained from untreated C33AE6-expressing cells show significant variations relating to increased and decreased peak intensities when compared to C33AV control cells (Fig. 4d). In Fig. 4a–c, several large changes were observed between the spectra of C33AE6 cells exposed to either indinavir (E6I) or lopinavir (E6L) when compared to untreated control cells. No peaks were seen at 670, 680, 746, 780 and 825 cm^{-1} in the spectrum of the C33AE6 cell, whereas the resulting spectra of these cells following the treatment with both compounds revealed marked signals at these wavenumber shifts. Interestingly, the peaks at 670, 780 and 825 cm^{-1} for E6I, and 680, 746 and 825 cm^{-1} for E6L, correspond to peaks typically ascribed to nucleic acids (Table 1). In contrast, no clear bands are observed at 1,063, 1,132 and 1,172 cm^{-1} in drug-treated C33AE6 cells, but which are very prominent in untreated C33AE6 cells. This also suggests an additional phenotypic effect as these can be attributed to the reduction in proteins, lipids and aromatic amino acids (Table 1). These spectral differences between the C33AE6 and drug-treated C33AE6 cells are

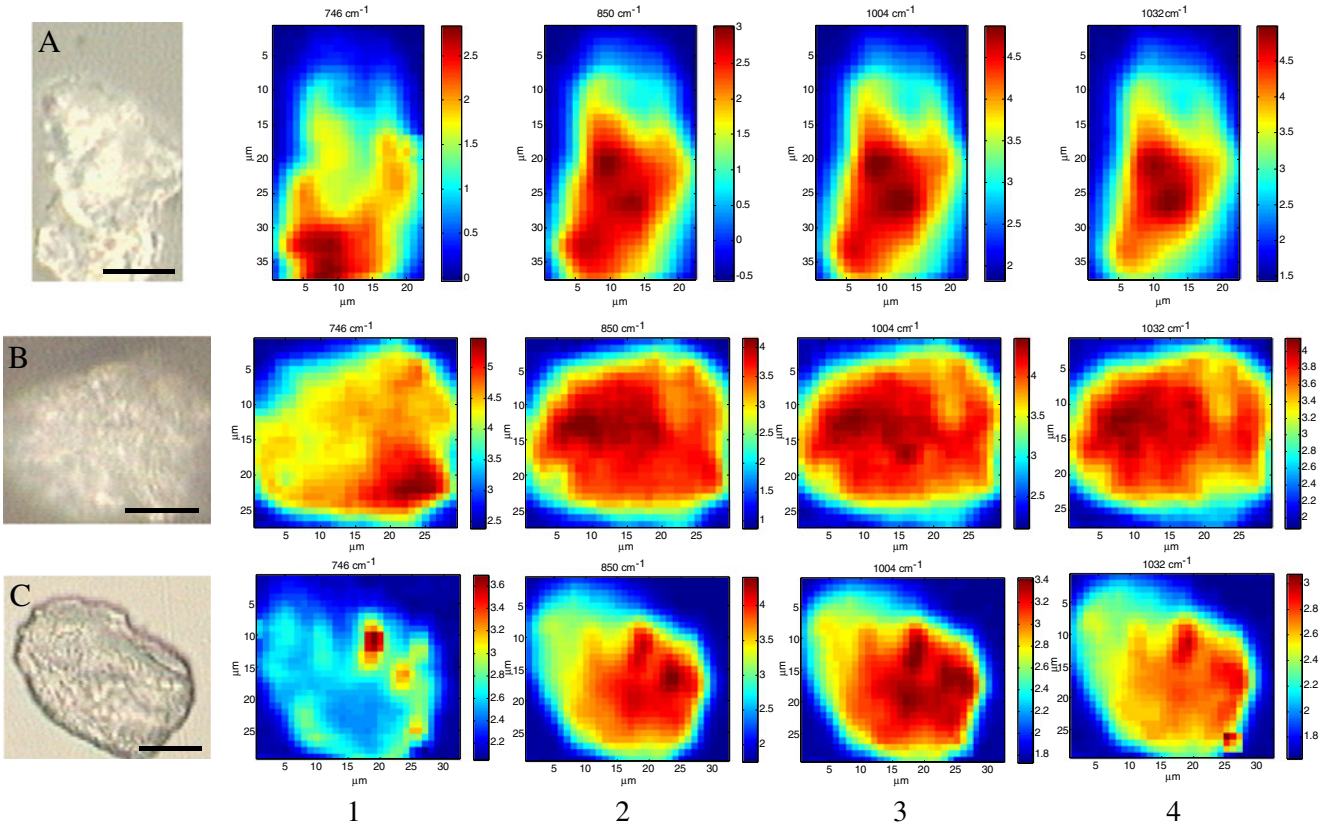

Fig. 3 White light images of C33A vector control cell (**a**), vector cell exposed to indinavir (**b**) and vector cell exposed to lopinavir (**c**). *Scale bar*, 10 μm. Raman chemical mean filtered maps of each of these cells are also shown based on the results from each band of a mean row normalised spectrum with a spatial resolution of 1 μm: *1* 746 cm^{-1} (thymine); *2* 850 cm^{-1} (protein); *3* 1,004 cm^{-1} (phenylalanine); *4* 1,032 cm^{-1} (protein). The *rainbow maps* indicate the concentration of each cellular component inside the cell, *red* showing high and *blue* showing low concentration of molecules

not from the sample matrix effects as we have recently shown that the drugs cause changes in the levels of p53 protein [9] and intracellular metabolites [10] in cultured C33AE6, but not in C33AV cells. In addition, a very interesting feature of the E6I spectra is the band at 880 cm^{-1}. By comparing the spectrum of E6I to that of the drug itself (Fig. 4e), this was deduced to be a peak originating from indinavir itself. No discernible signal was observed associated with chemical detection of lopinavir within the cells.

White light and Raman spectra chemical image maps of untreated C33AE6 and drug-treated cells were acquired using the same instrumental conditions as those applied to C33AV cells (Fig. 5). As shown previously, vibrations arising from proteins are uniformly distributed throughout both E6I (642 cm^{-1}, 5B1; 1,003 cm^{-1}, 5B4; 1,088 cm^{-1}, 5B5) and E6L (1,003 cm^{-1}, 5 C4; 642 cm^{-1}, 5 C1; 850 cm^{-1}, 5B3). The chemical image maps of the drug-exposed C33AE6 cells show very interesting features in terms of the spatial distribution of nucleic acids. Unlike C33AV (Fig. 3) and untreated C33AE6 cells (Fig. 5a), there are clear localisations from 780 cm^{-1} for E6I to 747 cm^{-1} for E6L, as shown in 2 of Fig. 5b, c, respectively. Also, the maps from 670 to 825 cm^{-1} for E6I and 680 cm^{-1} for E6L show the same distinct localisations as 780 and 747 cm^{-1}, respectively (data not shown). Interestingly, all these wavenumbers which have distinct distributions are assigned to nucleic acids (Table 1).

LC-MS analysis of subcellular localisation of drug

LC-MS is a commonly used analytical approach within the metabolomics field [21] and was applied here to quantify the level of indinavir within nuclear and cytoplasmic extracts from indinavir-treated C33AE6 cells. Immunoprobing Western blots of these extracts with GAPDH and HDAC1 antibodies demonstrated minimal nuclear/cytoplasm cross-contamination (Fig. 6). Six biological replicates were analysed in triplicate by LC-MS for both nuclear and cytoplasmic extracts (Table 2). White light microscopy was used to determine the average relative volume of the cytoplasm *vs.* nucleus of indinavir-treated C33AE6 cells and was calculated as 11.6.

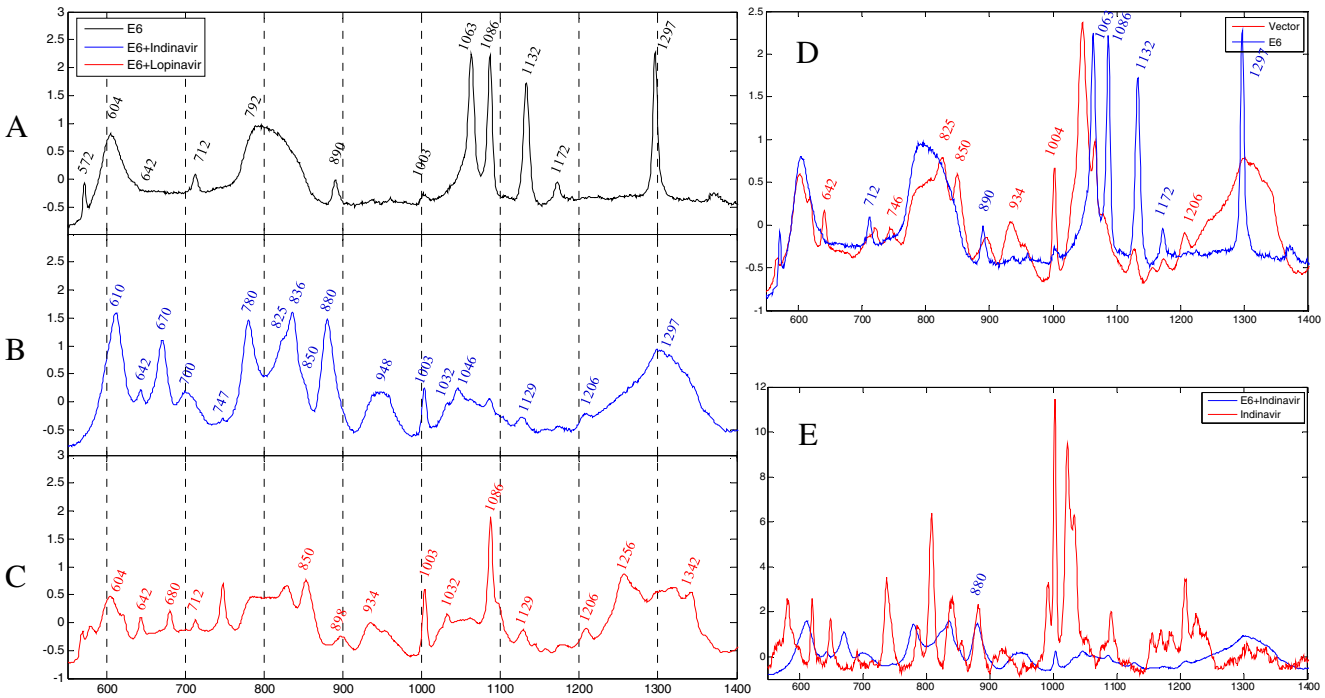

Fig. 4 Mean normalised spectra from C33AE6 cell (**a**) and E6 cells exposed to indinavir (**b**) and lopinavir (**c**). **d** Comparison of average Raman spectrum from E6 cell with that from vector control cell. **e** Comparison of average Raman spectra from indinavir exposed E6 cell with that from indinavir itself

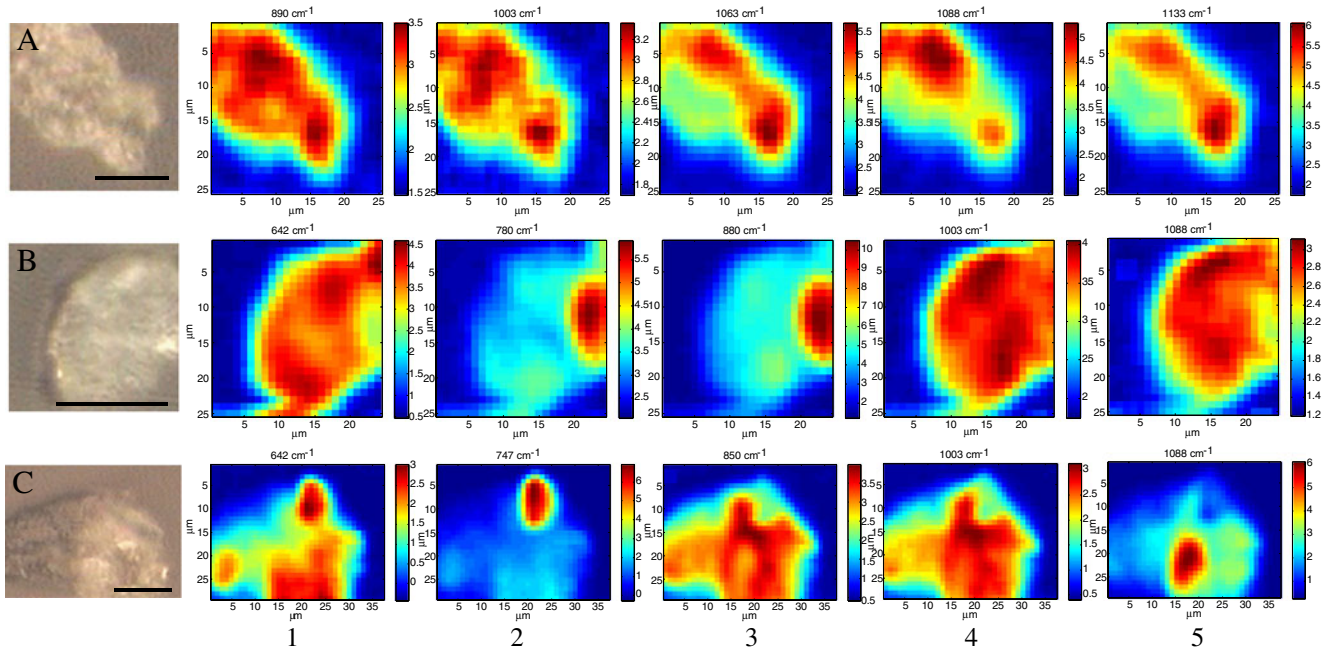

Fig. 5 White images of C33A E6 cell (**a**), E6 cell exposed to indinavir (**b**) and E6 cell exposed to lopinavir (**c**). *Scale bar*, 10 μm. Raman chemical mean filtered maps of each of these cells are also shown based on the results from each band of a mean row normalised spectrum with a spatial resolution of 1 μm. **a** *1* 890 cm^{-1} (nucleotide); *2* 1,003 cm^{-1} (phenylalanine); *3* 1,063 cm^{-1} (protein); *4* 1,088 cm^{-1} (nucleotide, protein); *5* 1,133 cm^{-1} (protein, lipid). **b** *1* 642 cm^{-1} (tyrosine); *2* 780 cm^{-1} (nucleotide); *3* 880 cm^{-1}; *4* 1,003 cm^{-1}; *5* 1,088 cm^{-1}. **c** *1* 642 cm^{-1}; *2* 747 cm^{-1} (nucleotide); *3* 850 cm^{-1} (protein); *4* 1,003 cm^{-1}; *5* 1,086 cm^{-1}. The *rainbow maps* indicate the concentration of each cellular component inside the cell, *red* showing high and *blue* showing low concentration of molecules

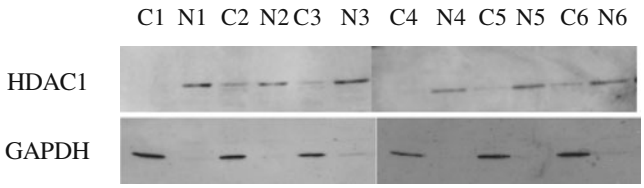

Fig. 6 Western blot of sub-fractionated samples from C33A E6-transfected cells exposed to indinavir and immunoprobed with a HDAC1 (nuclear marker) and GAPDH loading control antibodies. Sub-fractionation of drug-treated C33AE6 cells was carried out successfully with only minimal cross-contamination. *C* cytoplasm, *N* nuclear, *1–6* biological replicates

Discussion

Based on our previous studies of the effects of HIV PIs on the survival and metabolism of cultured cervical carcinoma cells [9, 10], we initially analysed the Raman spectra of HPV-negative C33A cells exposed to these drugs.

Raman spectroscopy is an optical approach in which a laser is used to irradiate a sample. Molecules within the sample vibrate, and this results in a change in energy of the light that can be measured and displayed as a Raman spectrum. This spectrum relates directly to the chemical composition of the sample [22].

The chemical mapping approach of Raman microspectroscopy involves coupling an optical microscope with a Raman spectrometer, and it is a powerful tool for analysing the chemical distribution of metabolites present at any point and the response of metabolic and physical stresses in cells or tissues [23]. Subtle changes in chemical composition and distribution on cells or tissues can be monitored using this Raman spectroscopic approach. This chemical mapping technique not only enables visualisation of spatially resolved chemical information but can also be used to detect small chemical changes in order to understand abiotic perturbations to biological systems. Thus, Raman spectroscopy has emerged as a promising diagnostic tool for disease detection in the biomedical field. Various diseases have been detected by comparing the differences of Raman spectra between normal and diseased cells or tissues because disease progression results in changes of the composition and abundance of metabolites [24–27]. The biomedical application of spectroscopy for cancer detection and disease diagnosis has been thoroughly reviewed in [22, 28, 29]. Finally, in order to develop effective chemotherapeutic agents and assess combinations of various drugs against serious diseases, the response to chemotherapy and the distribution of drugs inside cells or tissues have also been investigated [30, 31].

As can be seen in Fig. 2a–c, the differences between the spectra of drug-treated and control untreated C33AV cells are very subtle, apart from a large 1,047 cm^{-1} carbohydrate signal (see Table 1) which was reduced after incubation with either of the compounds. Although C33AV cells treated with lopinavir do not proliferate [9], the spectral differences from the level changes in intracellular components such as lipid, protein, DNA and RNA caused by proliferation are very subtle [32]. Therefore, the spectral changes between drug-challenged and non-drug-challenged control C33AV cells were not observed by visual analysis of vibrational bands in the Raman spectra.

Using these Raman spectral assignments, we next employed chemical mapping of drug-treated and control untreated C33AV cells in order to analyse intracellular distribution of internal components within the cells (Fig. 3). It is well known that biological molecules are not homogeneously distributed inside cells with localised and specific activities being related to their spatial distribution [33]. Raman chemical maps obtained from the average spectra of untreated and drug-treated C33AV cells show that the concentrations of different molecules show subcellular variation. Single cell image maps of proteins at 850, 1,004 and 1,032 cm^{-1} show a uniform distribution throughout the whole cell, whereas, as expected, the 746 cm^{-1} nucleic acid signal shows a more concentrated intracellular localisation that is consistent with specific nuclear compartmentalisation. Curiously, no Raman spectral bands that could be directly attributed to either of the drug compounds were observed in C33AV cells.

Following on from this, we investigated whether the expression of the E6 protein caused any discernible effects on the Raman spectral analysis. It is well known that E6, in association with E6AP, can facilitate the proteasomal destruction of numerous proteins, such as p53, that are detrimental to viral persistence [19]. Yet it is also known that the levels of other cellular proteins are increased by indirect effects of E6 and other viral proteins in HPV-infected cells [34, 35]. What is clear is that infection with

Table 2 Biological replicates of indinavir-treated C33E6 cells analysed in triplicate by LC-MS for both nuclear and cytoplasmic extracts

Fraction[a]	Cytoplasm abundance[b]	Nucleus abundance	Nucleus: cytoplasm
1	19.2	149.9	7.8
2	19.7	204.6	10.4
3	20.8	191.8	9.2
4	18.4	156.8	8.5
5	24.7	126.6	5.1
6	27.0	171.7	6.3
Mean			7.9

[a] Each fraction was analysed in triplicate (2 μL injected into LC-MS) and means are shown

[b] Abundance is the extracted ion chromatogram for the identified indinavir peak following scaling factors due to extraction volume differences and cytoplasm-to-nucleus volume

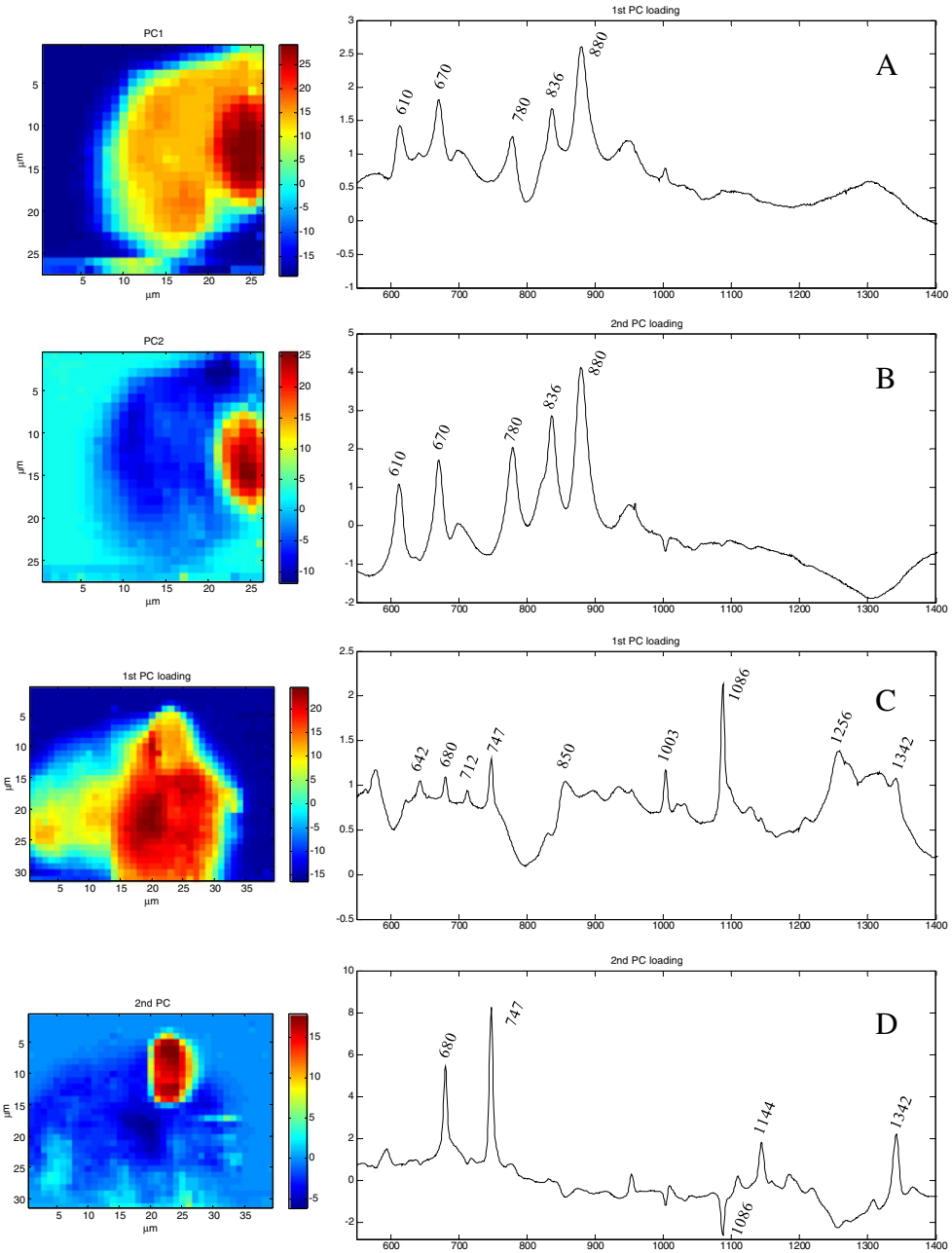

Fig. 7 PCA chemical maps constructed from PC scores with the corresponding loadings plots. E6-transfected cell exposed to indinavir showing PC1 (78.5%) (**a**) and PC2 (14.4%) (**b**) and E6-transfected cell exposed to lopinavir showing PC1 (85.6%) (**c**) and PC2 (6.5%) (**d**)

high-risk HPV produces multifactorial effects generally aimed at targeting and perturbing the function of a variety of cellular "hub" proteins. Thus, the spectral comparison of C33AV and E6 cells shown in Fig. 4d represents a snapshot of some of these effects which reflect the changes in the levels of cellular components. Indeed it is noteworthy that we have previously shown the biological properties of these two cell types to be very different. For example, xenografted experimental tumours derived from C33AE6 cells are highly resistant to radiotherapy when compared to tumours derived from C33AV cells [12], and more recently, we have used the complementary vibration technique of FT-IR spectroscopy to elucidate gross phenotypic differences between control C33A cells and those expressing E6 [10].

If lopinavir or indinavir can specifically target the biological effects of E6, we hypothesised that treatment of C33AE6 cells with these compounds may induce associated alterations in the Raman spectra. Indeed, we found large variations in the spectra between untreated and drug-treated C33AE6 cells (Fig. 4) which corresponded to peaks arising from nucleic acids and other components such as proteins, lipids and aromatic amino acids. With regard to the function of E6, it could be speculated that these drugs might increase

the level of specific types of nucleic acids in cells, and it is intended to continue work on this effect by the use of metabolic profiling [36].

To determine whether there was any difference between drug-treated and untreated C33AE6 cells in terms of the biochemical distribution of intracellular components, Raman chemical maps of these cells were generated. As can be seen in Fig. 5, although proteins are uniformly distributed within both untreated and drug-treated E6 cells, distinct localisation of nucleic acids was observed in drug-treated C33AE6 cell. Based upon the comparison of the spatial co-localisation of nucleic acids with that of the prospective indinavir signal at 880 cm^{-1}, it is possible that the metabolic activity of this drug against E6 may occur in the nucleus.

In order to investigate this hypothesis further, PCA of drug-exposed (E6I and E6L) cells was conducted. PCA provides the most compact representation of all the variations within the multivariate datasets by visualising and mining information from an XY data matrix containing the large number of Raman-detected variables (in the *Z*-axis in this spectral hypercube). Thus, in order to investigate which spatial region is the most variable and which spectral band is related to the area, PCA was carried out as described above. PCA chemical maps and their loadings plots are shown in Fig. 7. The maps and loadings plots from the PCA allow for the selection of significant variables associated with the drug activities from the spectrum of each cell. For C33AE6 cell exposed to indinavir, 78.5% of the total explained variance was recovered in the first PC and 14.4% in the second PC, whilst for C33AE6 cell exposed to lopinavir, PC1 accounted for 85.6% and PC2 6.5%. For these indinavir and lopinavir exposures, the total for the first two PCs was 92.9% and 92.1%, respectively, which highlights the efficient dimensionality reduction that PCA has achieved. On the basis of chemical image maps and loadings plots from PC1 to PC2 (representing the largest and second largest variations, respectively), many of the important variations occurring in E6I cells are found to be associated with peaks at 670, 780 and 836 cm^{-1} corresponding to nucleic acids (Fig. 7a, b). Furthermore, the large variation of the band at 880 cm^{-1} indicates that the drug location is related to changes in the levels of nucleic acids which may occur in the nucleus. For both E6I and E6L, it was found that the largest variations (PC1) were derived from nucleic acids, although a large contribution was also made by proteins. The second largest variations (PC2) mostly occurred at the position corresponding to peaks arising from the following nucleic acid signals: 680, 747 and 1,432 cm^{-1} (Fig. 7c, d).

In order to support the hypothesis that indinavir localises to the nucleus, we evaluated its levels in drug-treated sub-fractionated C33AE6 cells by the use of LC-MS. After taking into account the difference between the volume of the cytoplasm compared to the nucleus, LC-MS indicated that the concentration of indinavir was approximately eight-fold greater in the nucleus than in the cytoplasm of these cells (Table 2). Clearly, this orthogonal analytical technique definitively confirms the findings from Raman chemical mapping that indinavir is being localised to the nucleus of E6-expressing cells, and this is presumably the site of action for this antiviral drug.

Conclusions

We have used Raman chemical image mapping to compare the distribution of intracellular components within human C33A cervical cancer cells and the same cells expressing the HPV16 E6 oncoprotein. Significant variations were observed between the spectra of these two cell types, which indicates that the expression of E6 induces gross phenotypic changes which are consistent with our previous FT-IR spectroscopy-based study [10]. Finally, we also have unequivocal evidence that the HIV antiviral drug indinavir is specifically targeted to the nucleus of HPV16 E6-expressing cervical carcinoma cells. This unexpected finding will facilitate the analysis of potential drug targets for this prospective novel use of this class of compound.

Acknowledgements This research was funded by an ORS award to D-H.K. R.M.J. is very thankful to the UK BBSRC for funding. J.W. A., E.M.-E. and R.G. are grateful to the EU-funded project, Metabolomics for Plants Health and OutReach (META-PHOR: FOOD-CT-2006-036220), for financial support. R.G. is grateful to both the UK BBSRC and EPSRC for financial support of the MCISB. The authors also acknowledge the support of the Humane Research Trust, the Caring Cancer Research Trust and Cancer Research UK.

Disclosure statement The authors have no conflict of interest

References

1. zur Hausen H (1996) Papillomavirus infections—a major cause of human cancers. Biochim Biophys Acta 1288:55–78
2. de Villiers EM (1989) Heterogeneity of the human papillomavirus group. J Virol 63:4898
3. Scheffner M, Werness BA, Huibregtse JM, Levine AJ, Howley PM (1990) The e6 oncoprotein encoded by human papillomavirus types 16 and 18 promotes the degradation of p53. Cell 63:1129–1136
4. Harper DM, Franco EL, Wheeler C, Ferris DG, Jenkins D, Schuind A, Zahaf T, Innis B, Naud P, De Carvalho NS, Roteli-Martins CM, Teixeira J, Blatter MM, Korn AP, Quint W, Dubin G (2004) Efficacy of a bivalent l1 virus-like particle vaccine in prevention of infection with human papillomavirus types 16 and 18 in young women: a randomised controlled trial. Lancet 346:1757–1765
5. Munoz N, Bosch FX, de Sanjose S, Herrero R, Castellsague X, Shah KV, Snijders PJF, Meijer CJLM (2003) Epidemiologic

classification of human papillomavirus types associated with cervical cancer. N Engl J Med 348:518–527
6. Villa LL, Costa RLR, Petta CA, Andrade RP, Ault KA, Giuliano AR, Wheeler CM, Koutsky LA, Malm C, Lehtinen M, Skjeldestad FE, Olsson SE, Steinwall M, Brown DR, Kurman RJ, Ronnett RM, Stoler MH, Ferenczy A, Harper DM, Tamms GM, Yu J, Lupinacci L, Railkar R, Taddeo FJ, Jansen KU, Essser MT, Sings HL, Saah AJ, Barr E (2005) Prophylactic quadrivalent human papillomavirus (types 6, 11, 16, and 18) l1 virus-like particle vaccine in young women: a randomised double-blind placebo-controlled multicentre phase II efficacy trial. Lancet Oncol 6:271–278
7. Kyrgiou M, Koliopoulos G, Martin-Hirsch P, Arbyn M, Prendiville W, Paraskevaidis E (2006) Obstetric outcomes after conservative treatment for intraepithelial or early invasive cervical lesions: systematic review and meta-analysis. Lancet 367:489–498
8. zur Hausen H (2000) Papillomaviruses causing cancer: evasion from host-cell control in early events in carcinogenesis. J Natl Cancer Inst 92:690–698
9. Hampson L, Kitchener HC, Hampson IN (2006) Specific HIV protease inhibitors inhibit the ability of hpv16 e6 to degrade p53 and selectively kill e6-dependent cervical carcinoma cells in vitro. Antivir Ther 11:813–825
10. Kim D-H, Jarvis RM, Xu Y, Oliver AW, Allwood JW, Hampson L, Hampson IN, Goodacre R (2010) Combining metabolic fingerprinting and footprinting to understand the phenotypic response of hpv16 e6 expressing cervical carcinoma cells exposed to the hiv anti-viral drug lopinavir. Analyst 135:1235–1244
11. Chow WA, Jiang C, Guan M (2009) Anti-HIV drugs for cancer therapeutics: back to the future? Lancet Oncol 10:61–71
12. Hampson L, El Hady E, Moore JV, Kitchener H, Hampson IN (2001) The HPV16 e6 and e7 proteins and the radiation resistance of cervical carcinoma. FASEB J 15:1445–1447
13. Wold H (1966) Multivariate analysis. Academic, New York
14. Jolliffe IT (1986) Principal component analysis. Springer, New York
15. Sumner LW, Mendes P, Dixon RA (2003) Plant metabolomics: large-scale phytochemistry in the functional genomics era. Phytochemistry 62:817–836
16. Laemmli UK (1986) Cleavage of structural proteins during the assembly of the head of bacteriophage T4. Nature 227:680–685
17. Wrona M, Mauriala T, Bateman KP, Mortishire Smith RJ, O'Connor D (2005) All-in-one analysis for metabolite identification using liquid chromatography/hybrid quadrupole time-of-flight mass spectrometry with collision energy switching. Rapid Commun Mass Spectrom 19:2597–2602
18. Bateman KP, Castro-Perez J, Wrona M, Shockcor JP, Yu K, Oballa R, Nicoll-Griffith DA (2007) Ms^e with mass defect filtering for in vitro and in vivo metabolite identification. Rapid Commun Mass Spectrom 2:1485–1496
19. Banks L, Pim D, Thomas M (2003) Viruses and the 26S proteasome: hacking into destruction. Trends Biochem Sci 28:452–459
20. Mantovani F, Banks L (1999) The interaction between p53 and papillomaviruses. Semin Cancer Biol 9:387–395
21. Allwood JW, Goodacre R (2010) An introduction to liquid chromatography–mass spectrometry instrumentation applied in plant metabolomic analyses. Phytochem Anal 21:33–47
22. Ellis DI, Goodacre R (2006) Metabolic fingerprinting in disease diagnosis: biomedical applications of infrared and Raman spectroscopy. Analyst 131:875–885
23. Clark D, Sasic S (2006) Chemical images: technical approaches and issues. CytometryA 69a:815–824
24. Buschman HP, Deinum G, Morz JT, Fizmaurice M, Kramer JR, van der Laarse A, Bruschke AV, Feld MS (2001) Raman microspectroscopy of human coronary atherosclerosis: biochemical assessment of cellular and extracellular morphologic structures in situ. Cardiovasc Pathol 10:69–82
25. Harris AT, Lungari A, Needham CJ, Smith SL, Lones MA, Fisher SE, Yang XB, Cooper N, Kirkham J, Smith DA, Martin-Hirsch DP, High AS (2009) Potential for Raman spectroscopy to provide cancer screening using a peripheral blood sample. Head Neck Oncol 1:34–41
26. Hawi SR, Campbell WB, Balla AK, Murphy R (1996) Characterization of normal and malignant human hepatocytes by Raman microspectroscopy. Cancer Lett 110:35–40
27. Shafer-Peltier KE, Haka AS, Fitzmaurice M, Crowe J, Myles J, Dasari RR, Feld MS (2002) Raman microspectroscopic model of human breast tissue: implications for breast cancer diagnosis in vivo. J Raman Spectrosc 33:552–563
28. Ellis EI, Dunn WB, Griffin JL, Allwood JW, Goodacre R (2007) Metabolic fingerprinting as a diagnostic tool. Pharmacogenomics 8:1243–1266
29. Mahadevan-Jansen A, Richards-Kortum R (1997) Raman spectroscopy for cancer detection: a review. Conf Proc IEEE Eng Med Biol Soc 6:2722–2728
30. Beljebbar A, Sockalingum GD, Morjani H, Manfait M (1999) Raman and sers microspectroscopy on living cells: a promising tool towards cellular-drug response and medical diagnosis. Proc SPIE 3608:175–184
31. Kang E, Wang H, Kwon IK, Robinson J, Park K, Cheng JX (2006) In situ visualization of paclitaxel distribution and release by coherent anti-stokes Raman scattering microscopy. Anal Chem 78:8036–8043
32. Short KW, Carpenter S, Freyer JP, Mourant JR (2005) Raman spectroscopy detects biochemical changes due to proliferation in mammalian cell cutures. Biophys J 88:4274–4288
33. Uzunbajakava N, Lenferink A, Kraan Y, Willekens B, Vrensen G, Greve J, Otto C (2003) Nonresonant raman imaging of protein distribution in single human cells. Biopolymers 72:1–9
34. Wan F, Miao X, Quraishi I, Kennedy V, Creek KE, Pirisi L (2008) Gene expression changes during HPV-mediated carcinogenesis: a comparison between an in vitro cell model and cervical cancer. Int J Cancer 123:32–40
35. Martin CM, Astbury K, McEvoy L, O'Toole S, Sheils O, O'Leary JJ (2009) Gene expression profiling in cervical cancer: identification of novel markers for disease diagnosis and therapy. Meth Mol Biol 511:333–359
36. Goodacre R, Vaidyanathan S, Dunn WB, Harrigan GG, Kell DB (2004) Metabolomics by numbers: acquiring and understanding global metabolite data. Trends Biotechnol 22:245–252
37. Faolain EO, Hunter MB, Byrne JM, Kelehan P, Byrne HJ, Lyng FM (2005) The potential of vibrational spectroscopy in the early detection of cervical cancer: an exciting emerging field. Proc SPIE 5826:25–36
38. Notingher IN, Verrier S, Haque S, Polak JM, Hench LL (2003) Spectroscopic study of human lung epithelial cells (a549) in culture: living cells versus dead cells. Biopolymers 72:230–240